Over-85-GHz-Bandwidth InP-Based Coherent Driver Modulator Capable of 1-Tb/s/λ-Class Operation

Josuke Ozaki, Yoshihiro Ogiso, *Member, IEEE*, Yasuaki Hashizume, Hiroshi Yamazaki, *Member, IEEE*, Kazuya Nagashima, *Member, IEEE*, Nobuhiro Nunoya, *Member, IEEE*, and Mitsuteru Ishikawa, *Member, IEEE*

(Invited Paper)

***Abstract*—We developed an InP-based coherent driver modulator (CDM) with a flexible printed circuit (FPC) RF interface. The CDM has a 3-dB electro-optic (EO) bandwidth of over 85 GHz, including the evaluation board loss, which is sufficient for 1-Tb/s/λ-class operation. Furthermore, we obtained good back-to-back bit-error-rate (BER) performance in modulations up to 144-Gbaud dual-polarization 16-QAM, and we confirmed the CDM's capability for operation over the 150-Gbaud class. With the FPC RF interface, a package's roll-off frequency above 100 GHz was demonstrated in both measured and simulated results. The CDM includes an InP-based n-i-p-n heterostructure modulator chip with a differential capacitively loaded traveling-wave electrode (CL-TWE) and a 4-channel linear SiGe BiCMOS driver IC with an open-collector configuration and low wire inductance. The modulator chip has an EO 3-dB bandwidth of over 70 GHz, which is an improvement of about 30 GHz over that of a conventional p-i-n structure. In addition, to facilitate future 200-Gbaud-class operation, a simulation with a reduced GND via diameter confirmed that the package's roll-off frequency can be improved to more than 120 GHz. Moreover, by reducing the CL-TWE period and the metal's DC resistance, the n-i-p-n modulator chip achieve an EO 3-dB bandwidth of 90 GHz or more.**

***Index Terms*—Digital coherent, electrooptic modulation, flexible printed circuit, high-speed optical modulators, indium compounds, quadrature amplitude modulation.**

I. Introduction

INTERNET traffic continues to grow year after year because of the spread of telework, the increased usage of video streaming services, and so on. Constant growth in the optical capacity of optical transmission systems will be essential to maintain the quality of the optical networks. Higher symbol rates and higher-order modulation formats are important techniques to increase the transmission capacity per wavelength [1], [2], [3].

Optical devices for digital coherent optical transceivers, such as a coherent driver modulator (CDM) [4], [5], [6] and an intradyne coherent receiver (ICR) [6], [7], [8], are key components for high-speed multi-level operation. These components integrate optical and electrical devices in one package to reduce the RF loss, footprint and cost. In the CDM, a Mach-Zehnder modulator chip and a linear driver are placed adjacent to each other. Similarly, in the ICR, a photodiode and a linear transimpedance amplifier are adjacent. In the CDM case, standardization is complete for operation up to 128-Gbaud with a 3-dB electro-optic (EO) bandwidth above 75 GHz, called Class 80 [4].

InP modulator chips have been commonly used for CDMs [5], [6] because they can achieve high bandwidth with a low driving voltage and a small footprint [9], [10]. Recently, novel CDM using a thin-film $LiNbO_3$ (TFLN) modulator was demonstrated [11]. TFLN modulators are very promising for the next generation of high-speed modulators because of their small footprint, low half-wave voltage (V_π), and high bandwidth [12], [13], [14], [15]. InP and TFLN modulators can achieve almost the same excellent characteristics. In contrast, silicon photonics (SiPh) modulators are currently inferior in terms of both the V_π and bandwidth [16], [17]. It is thus difficult to apply SiPh modulators in CDMs, which are used for high-end transceivers.

Although TFLN modulator chips with excellent performance have been reported at the laboratory level, there have been very few reports of packaged TFLN modulators, and their market introduction as optical transceivers has made little progress. We believe that this is partly due to their single-ended drive configuration [15]. To achieve high signal integrity and efficient connection between the modulator chip and the driver IC, each component should have a differential drive configuration [18], [19]. InP modulators with a single-ended drive scheme were previously popular [20], [21], [22], but they now mainly use a differential drive scheme [9], [10].

Recently, we developed an InP-based CDM with a flexible printed circuit (FPC) RF interface. This CDM has an EO 3-dB bandwidth of over 80 GHz, and it demonstrated 128-Gbaud dual-polarization (DP) 16-quadrature amplitude modulation (QAM) operation [23]. This is the highest bandwidth of any CDM

Manuscript received 14 November 2022; revised 23 December 2022; accepted 10 January 2023. Date of publication 16 January 2023; date of current version 9 June 2023. *(Corresponding author: Josuke Ozaki.)*

Josuke Ozaki, Yoshihiro Ogiso, Yasuaki Hashizume, Nobuhiro Nunoya, and Mitsuteru Ishikawa are with the NTT Device Innovation Center, Nippon Telegraph and Telephone Corporation, Atsugi 243-0198, Japan (e-mail: josuke.ozaki.mp@hco.ntt.co.jp; yoshihiro.ogiso.uv@hco.ntt.co.jp; yasuaki.hashizume.ph@hco.ntt.co.jp; nobu.nunoya.pm@hco.ntt.co.jp; mitsuteru.ishikawa.pe@hco.ntt.co.jp).

Hiroshi Yamazaki is with the NTT Device Technology Laboratories, Nippon Telegraph and Telephone Corporation, Atsugi 243-0198, Japan (e-mail: hiroshi.yamazaki.mt@hco.ntt.co.jp).

Kazuya Nagashima is with the Advanced Photonic Integrated Devices Development Department, Furukawa Electric Company, Ltd, Ichihara 290-8555, Japan (e-mail: kazuya6.nagashima@furukawaelectric.com).

Color versions of one or more figures in this article are available at https://doi.org/10.1109/JLT.2023.3236962.

Digital Object Identifier 10.1109/JLT.2023.3236962

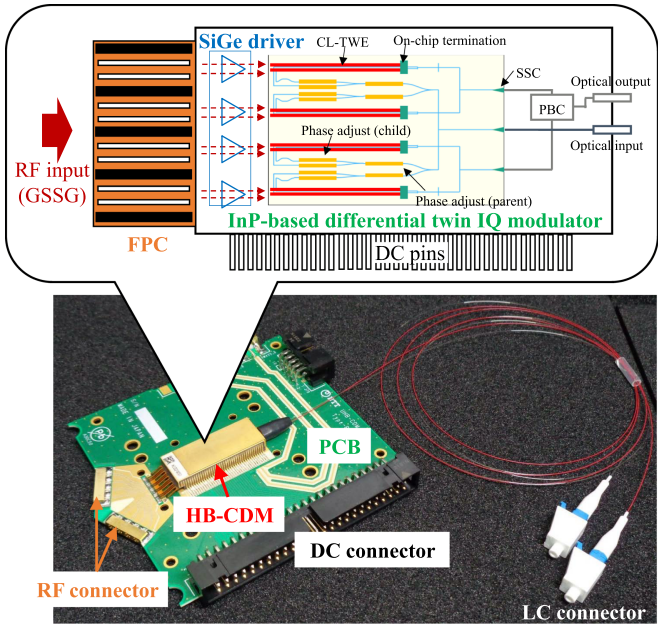

Fig. 1. Photograph and schematic diagram of the developed CDM.

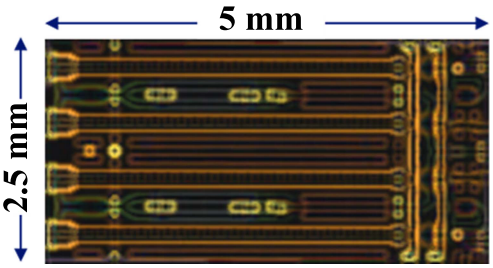

Fig. 2. Photograph of the fabricated modulator chip.

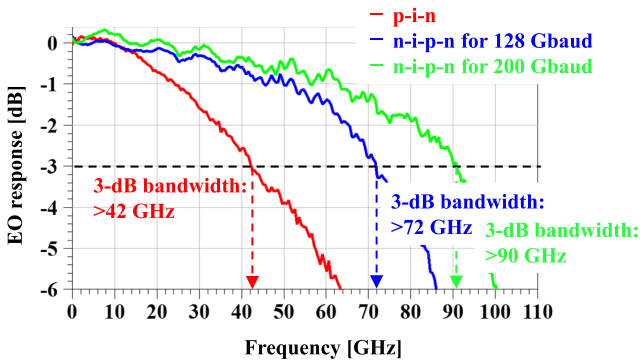

Fig. 3. Small-signal EO response of the InP-based modulator chip.

reported to date. The FPC package overcomes the bandwidth limitation in a surface-mount-type (SMT) package, which is used in conventional CDMs [24], [25].

In this extended paper, we detail the RF design and characteristics of the modulator chip and the CDM in Sections II and III. We also report back-to-back bit-error-rate (BER) performance in modulations up to 144-Gbaud DP-16QAM.

II. Design of Coherent Driver Modulator

Fig. 1 shows a photograph and schematic diagram of the developed CDM with an FPC RF interface and an SMT DC interface. The FPC and lead pins were soldered to a printed circuit board (PCB) for evaluation, and the PCB's RF pads were designed to be differential 100 Ω when the FPC was soldered. The amount of solder for the RF connection was controlled because too much solder would cause impedance mismatch with a low impedance. The package body size is $12 \times 30 \times 5.3$ mm^3. The transparent coating fiber is a polarization-maintaining input fiber, and the red coating fiber is a single-mode output fiber, with each having an LC connector. The package includes an InP-based n-i-p-n heterostructure modulator chip with a differential capacitively loaded traveling-wave electrode (CL-TWE), and adjacent to a 4-channel linear SiGe BiCMOS driver IC with an open-collector configuration. This section describes the features and characteristics of each component.

A. InP-Based Mach-Zehnder Modulator

The developed twin-IQ modulator chip, which integrates four Mach-Zehnder interferometers (MZIs) in parallel, is shown in Fig. 2. The chip's footprint is 2.5×5.0 mm^2. It integrates a spot-size converter (SSC) [26] to stabilize the optical mode field and the lens coupling loss. A thermo-optic (TO) heater is used for DC phase adjustment. The on-chip optical insertion loss per polarization is less than 6.0 dB over the C-band, which is equivalent to or less than that of a commercial bulk-LN DP-IQ modulator [10]. The on-chip loss excludes the optical coupling loss of 2.3 dB/facet between the modulator chip and the lensed fiber (4.5-μm mode field diameter) and a polarization splitting loss of 3 dB. The chip's RF modulation region comprises an n-i-p-n heterostructure diode. The n-i-p-n structure allows the p-cladding layer to be very thin, which can greatly reduce the optical and RF losses as compared to the conventional p-i-n structure. The optical propagation loss in the RF region is about 1.1 dB/cm, which is approximately 40% less than that of the conventional p-i-n structures. Furthermore, except for the RF region, the top n-cladding layer is eliminated by an InP regrowth process to reduce the optical propagation loss to around 0.6 dB/cm, which is about half the loss of the RF region. As compared to DC phase adjustment using the EO effect, the TO heater is also advantageous in terms of the propagation loss because the top n-cladding layer can be removed

Fig. 3 compares the measured small-signal EO responses of the p-i-n (red) and n-i-p-n structures (blue) used for the 128-Gbaud-class CDM here, along with a novel next-generation chip (green) targeting a 200-Gbaud-class CDM. The chips have a differential CL-TWE and on-chip termination, which were designed to be differential 60 Ω. In general, a low-impedance RF design is desirable to achieve higher bandwidth, because the modulator chip has a trade-off between the impedance and RF loss. On the other hand, to increase an output amplitude of a driver IC and achieve deep modulation depth, a high-impedance modulator design is desirable. The impedance of 60 Ω was

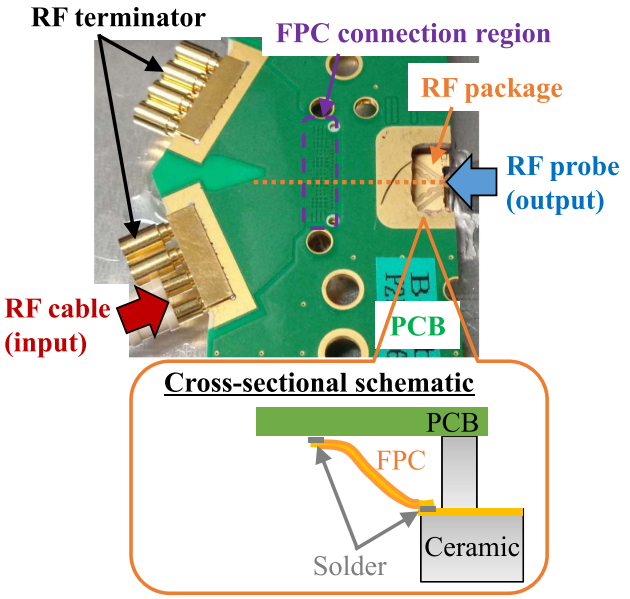

Fig. 4. Fabricated FPC package sample for RF measurement.

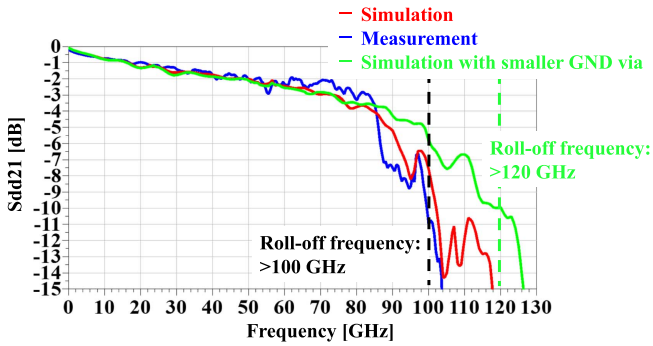

Fig. 5. Simulated and measured RF characteristics of the FPC package.

designed to ensure sufficient modulation depth when connected with an open-collector driver. The EO 3-dB bandwidth of the n-i-p-n structure for the 128-Gbaud class is over 72 GHz, which is an improvement by about 30 GHz over the conventional p-i-n structure's bandwidth. This is possible because the contact resistivity and cladding resistivity can be reduced to 1/10 or less than that of the p-i-n structure. The novel chip for a 200-Gbaud class CDM uses the same n-i-p-n structure. To achieve a higher bandwidth with same V_π of 2 V, the CL-TWE period was further reduced [9], and the metal's DC resistance was also lowered. The EO 3-dB bandwidth of the 200-Gbaud-class chip is more than 90 GHz, which is about 20 GHz better than that of the 128-Gbaud-class chip. The 3-dB bandwidth is the highest reported so far for an InP modulator a with a V_π of below 2 V.

B. Package

An SMT package has a roll-off frequency in the range of 70 to 80 GHz range because of the manufacturable minimum RF via dimensions and the impedance mismatch near the lead pins [25]. To avoid the SMT package's bandwidth limitation, we use an FPC as the RF interface. Fig. 4 shows a photograph and a cross-sectional image of a sample that we used to measure the package's RF characteristics. To evaluate these characteristics, including the soldering area between the FPC and PCB, the FPC package was soldered to the PCB with push-on RF connectors (G3PO). Moreover, the package and PCB were modified so that the RF probe could access the RF pads inside the package. The FPC comprises a double-sided structure with a 50 μm-thick polyimide-based core and 12.5-μm-thick polyimide-based coverlay films on both sides. The FPC is approximately 8.5 mm long and 11 mm width.

Fig. 5 shows simulated (red) and measured (blue) S-parameter results of the FPC package. These results include the losses of the connection area between the FPC and PCB and the 2.5-mm-long RF transmission line on the PCB from the edge of the FPC. Other RF losses, such as those from the transmission lines and the connector after the 2.5-mm RF line on the PCB, were de-embedded by using the test coupon's measurement results. The measured Sdd_{21} characteristic shows good agreement with the simulation result. The both simulated and measured results show a roll-off frequency of about 100 GHz, which is sufficient for a 128-Gbaud-class CDM. In addition, the green line in Fig. 5 shows the simulation result with smaller-diameter GND vias, which confirms an improvement of about 20 GHz in the roll-off frequency by downsizing and relocating the GND vias. With this improvement, the roll-off frequency can be increased to over 120 GHz, which demonstrates this FPC package has the potential for application in a 200-Gbaud-class CDM.

C. Assembly

For the driver IC, we use a SiGe BiCMOS 4-channel linear driver with no load resistors. The configuration, called open-collector, has the advantages of reducing power consumption and allowing an impedance of a modulator connected to the output stage of the driver to be freely set. A differential output amplitude of 2.5 V_{ppd} for differential 60 Ω and a power dissipation of 3.5 W or less at a case temperature of 75 °C. The 3-dB electrical bandwidth is 95 GHz or higher without considering wire inductance. The peaking frequency and peaking amount were around 70 GHz and 15 dB, respectively. However, in our CDM, all components (i.e., the package, driver IC, and modulator chip) are connected by ball wires. Therefore, it is important to design the total EO characteristics to account for connection wire inductance.

Fig. 6(a) shows the CDM's calculated EO response with a wire inductance of 50 (red), 100 (blue), or 150 (green) pH at the connection between the driver and the modulator chip. In these calculations, the connecting wire inductance between the package and driver was fixed at 100 pH. The simulation results show that changing the inductance from 50 pH to 150 pH leads to the approximately 10-GHz degradation in the EO 3-dB bandwidth. Fig. 6(b) shows the calculated EO response with a wire inductance between the package and driver of 50 (red), 100 (blue), or 150 (green) pH; here, the wire inductance

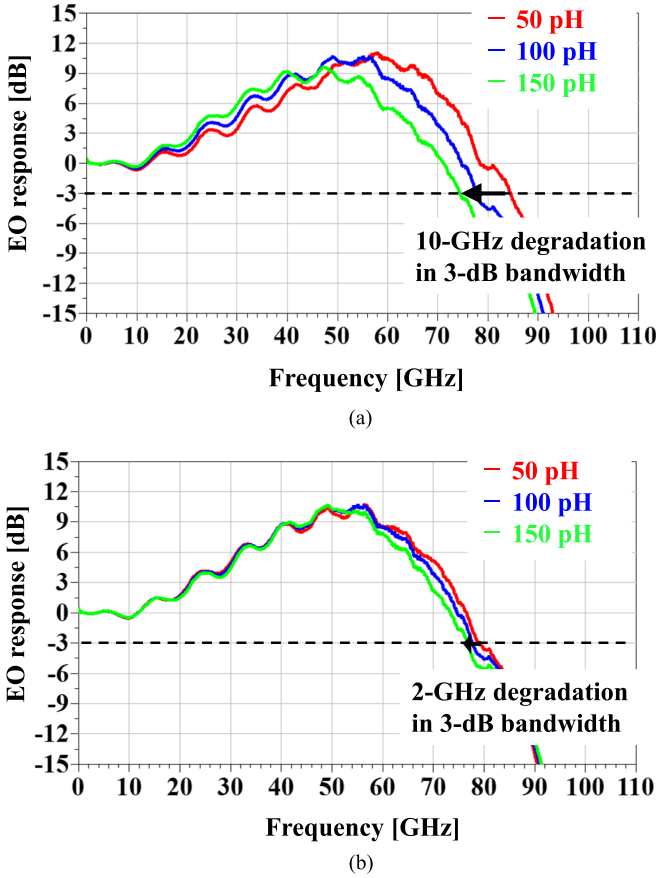

Fig. 6. Calculated EO response of the CDM with changing wire inductance values (a) Between the driver and modulator chip and (b) Between the package and driver.

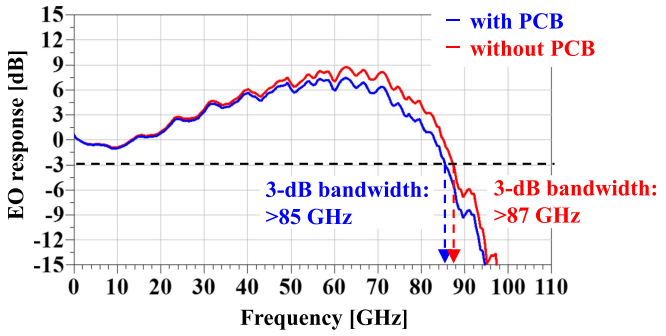

Fig. 7. Measured EO response of the developed CDM with and without the PCB.

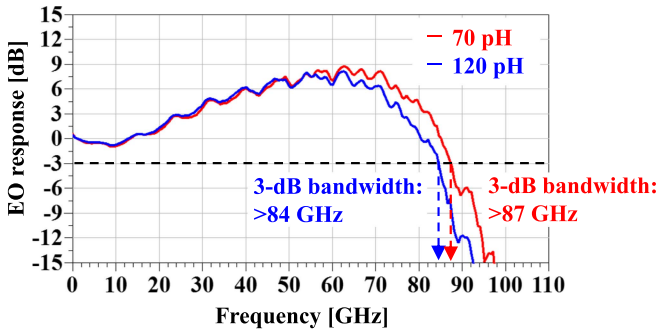

Fig. 8. Wire inductance dependence of the developed CDM's measured EO response without the PCB.

between the driver and modulator was fixed at 100 pH. In this case, the EO 3-dB bandwidth degradation is about 2 GHz when the wire inductance is changed from 50 pH to 150 pH. These results indicate that, to expand the CDM's bandwidth, low wire inductance is more important between the driver and modulator than between the package and driver.

Thus, to achieve low-inductance connections, we use double wires in parallel for each pad, and the gap between the driver and modulator chip is controlled to be around 30 μm. In addition, the heights between devices and the order of wire bonding are controlled by designing the wire ball height to minimize the wire loop length. Thermal management is also important to suppress the CDM's power consumption. The modulator chip is mounted on a thermoelectric cooler (TEC) for temperature control. As for the RF characteristics, shorter wires between the driver and modulator chip are desirable, however, from the standpoint of power dissipation, shorter wires result in greater heat inflow to the TEC and thus higher power consumption by the TEC. Accordingly, in our CDM, the wires on the RF side are shortened to ensure the appropriate RF characteristics; meanwhile, to suppress the heat inflow to the TEC, the wires on the DC side to connect the package and modulator are more than a few millimeters in length and less than 20 μm in diameter. Furthermore, the TEC's power consumption can be reduced with a higher TEC height, assuming that the element density and footprint are unchanged. The TEC in this CDM was thus designed to be as thick as possible.

III. Experimental Results

A. Small-Signal EO Response

Fig. 7 shows the fabricated CDM's measured small-signal EO response. The blue line represents the EO response including the evaluation board's RF loss, while the red line represents the EO response with de-embedding of the board loss after 2.5 mm from the FPC edge. With and without the board loss, the 3-dB bandwidth of the CDM is exceeding 85 GHz and 87 GHz, respectively. The bandwidth variation in either case is about 2 GHz. These are the highest EO 3-dB bandwidth values reported for any CDM to date. As seen in Fig. 7, the evaluation board's loss after 2.5mm from the FPC edge is about 2 dB at 80 GHz. These results confirm that the board loss was suppressed by using small RF connectors and making the transmission line as short as possible. This is less than half the board loss of a CDM reported previously [6].

Fig. 8 shows the wire inductance dependence of the measured EO response without the board loss. The red line represents the EO response with a wire inductance between the driver and modulator of 70 pH or less (same data as the red line in Fig. 7), while the blue line represents the response with a 120-pH wire inductance. In addition, a wire inductance between the

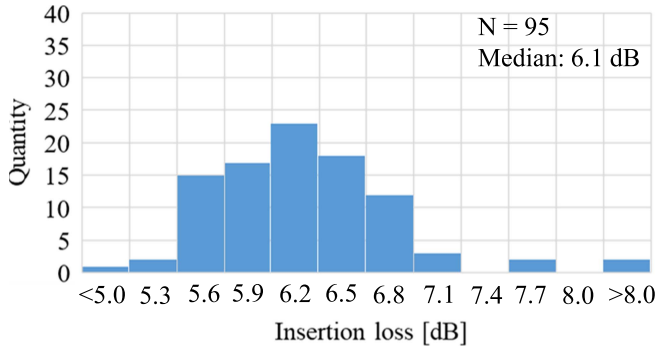

Fig. 9. Histogram of the optical insertion losses of 95 CDMs after combining X and Y polarization.

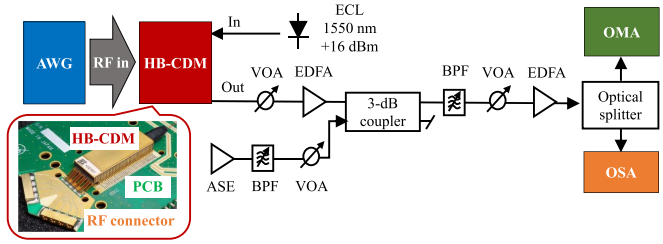

Fig. 10. Experimental setup for IQ modulations.

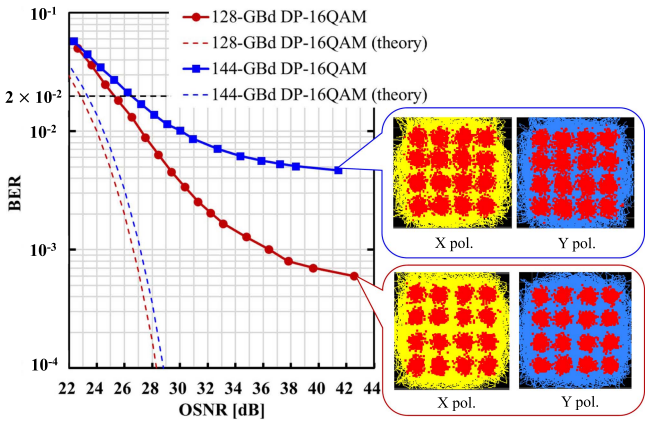

Fig. 11. BER characteristics and constellation diagram of 128-Gbaud DP-16QAM and 144-Gbaud DP-16QAM.

package and driver is about 100 pH. These inductance values were roughly estimated from the wire length. In the cases of 70 and 120 pH, the EO 3-dB bandwidths are over 87 GHz and 84 GHz, respectively. The 3-dB EO bandwidth change of about 3 GHz and the measurements here confirm that the wire inductance between the driver and modulator is very important for high bandwidth. To achieve a higher-bandwidth CDM, such as a 200-Gbaud-class CDM, the connection between the driver and modulator must have a lower inductance, which can be achieved by increasing the number of wire connections, using flip-chip bonding, and so on.

B. Optical Characteristics

Fig. 9 shows a histogram of the optical insertion loss (IL) of the maximum transmission at 1550 nm after combining X and Y polarization. This graph includes data collected from 95 prototypes. The median IL is about 6.1 dB, and the worst IL is about 8.5 dB, which indicates a low insertion loss and low variation. The median optical coupling loss between the modulator chip and the input/output fibers (including optical component losses such as those from a lens and a polarization beam combiner) was estimated to be around 3.0 dB. As for the polarization dependence loss (PDL), the median is about 0.13 dB, and the PDL was less than 0.3 dB in more than 80% of the samples. Even if the modulator chip does not integrate a PDL adjustment mechanism such as a variable optical attenuator (VOA) or a semiconductor optical amplifier (SOA), a very stable insertion loss variation between X and Y polarization can be achieved. This is due to the modulator chip's reduced on-chip loss via the n-i-p-n structure and the SSC's stable mode field. The low on-chip loss and the mode field stabilization by the input/output SSC which suppresses the optical coupling loss, thus result in a very low IL and PDL. In addition, the worst extinction ratio (ER) among the four child MZIs has a median value of about 33 dB, and the ER exceeded 30 dB in about 80% of the samples, which is a sufficient ER for 16-QAM or higher-order modulation formats.

C. IQ Modulation

Fig. 10 shows the experimental setup for back-to-back IQ modulations. The CDM used in this evaluation had a 3-dB EO bandwidth of over 80 GHz, an IL per polarization of 8 dB, and an ER (for both child and parent MZIs) of over 30 dB [23]. A light source with a line width of $<$100 kHz was used. The source's output power and wavelength were $+$16 dBm and 1550 nm, respectively. The RF signal source was a 256 GS/s arbitrary waveform generator (AWG) with a digital-analog converter (DAC) having a 3-dB analog bandwidth of about 70 GHz. An optical modulation analyzer (OMA) with a 3-dB analog bandwidth of $>$100 GHz was used at the receiver end. The RF signals were input by connecting the AWG and the RF connectors on the PCB via an RF cable with a total length of about 25 cm. An erbium-doped fiber amplifier (EDFA) and a variable optical attenuator (VOA) were used to adjust the optical signal power to a constant value. The received optical signal-to-noise ratio (OSNR) was controlled with an amplified spontaneous emission (ASE) noise source and a 5.5-nm band-pass filter (BPF). For the OSNR measurements, the optical output spectrum through a 3-nm BPF was measured by an optical spectrum analyzer (OSA).

Fig. 11 shows the back-to-back BER performance and the constellations for 128-Gbaud DP-16QAM (red) and 144-Gbaud DP-16QAM (blue) modulations. The AWG could output a maximum baud rate of 144 Gbaud. The dashed lines shows the theoretical BER curves. The OSNR was measured in a 0.1-nm reference noise bandwidth. The RF signals from the AWG were pulse-shaped with a root-raised-cosine (RRC) filter, and the roll-off factor and pseudorandom binary sequence (PRBS) length were 0.1 and $2^{15}-1$, respectively. The modulator bias was set to obtain a V_π of 2.0 V, and the driver gain at 1 GHz was

set to be differential 15 dB. The output optical power was −7 dBm, and the modulation loss was about 13 dB, excluding the quadrature 3-dB loss. This means that the modulation depth was about 35-40% in these measurements.

As seen in Fig. 11, the measured BERs at the best OSNR (about 42 dB) for the 128-Gbaud DP-16QAM and 144-Gbaud DP-16QAM are 6.0×10^{-4} and 4.7×10^{-3}, respectively. The required OSNRs for back-to-back 128 Gbaud DP-16QAM and 144 Gbaud DP-16QAM are 25.5 dB and 26.5 dB, respectively, below a pre-FEC BER threshold of 2×10^{-2}. In addition, there are OSNR deviations from the theoretical value of about 2.5 dB for 128-Gbaud DP-16QAM and about 3 dB for 144-Gbaud DP-16QAM. These results confirm that the developed CDM has sufficient characteristics for operation up to at least 144 Gbaud with the potential for operation over 150 Gbaud.

IV. Conclusion

We have developed a CDM with an FPC RF interface, which achieves an EO 3-dB bandwidth of over 85 GHz even with the evaluation board loss by using a low-inductance wire connection between the driver IC and modulator chip. We successfully demonstrated modulations up to 144-Gbaud DP-16QAM, and the CDM is capable of much higher baud rates. The CDM achieved the highest bandwidth reported to date, and it has the capability for 1-Tb/s/λ-class operations. Furthermore, we demonstrated a modulator chip with a 3-dB EO bandwidth of more than 90 GHz and showed the feasibility of a roll-off frequency of over 120 GHz in an FPC package, which should facilitate a CDM with the capability to achieve next-generation, 200-Gbaud-class operation.

References

[1] M. Nakamura et al., "Over 2-Tb/s net bitrate single-carrier transmission based on >130-GHz-bandwidth InP-DHBT baseband amplifier module," in *Proc. Eur. Conf. Opt. Commun.*, 2022, pp. 1–4.

[2] H. Mardoyan et al., "First 260-GBd single-carrier coherent transmission over 100 km distance based on novel arbitrary waveform generator and thin-film lithium niobate I/Q modulator," in *Proc. IEEE Eur. Conf. Opt. Commun.*, 2022, pp. 1–4.

[3] F. Pittalà et al., "1.71 Tb/s single-channel and 56.51 Tb/s DWDM transmission over 96.5 km field-deployed SSMF," *IEEE Photon. Technol. Lett.*, vol. 34, no. 3, pp. 157–160, Feb. 2022, doi: 10.1109/LPT.2022.3142538.

[4] "Implementation agreement for the high bandwidth coherent driver modulator (HB-CDM)," OIF Implementation Agreement No. OIF-HB-CDM-02.0, 2021. [Online]. Available: https://www.oiforum.com/wp-content/uploads/OIF-HB-CDM-02.0.pdf

[5] J. Ozaki et al., "500-Gb/s/λ operation of ultra-low power and low-temperature-dependence InP-based high-bandwidth coherent driver modulator," *J. Lightw. Technol.*, vol. 38, no. 18, pp. 5086–5091, Sep. 2020, doi: 10.1109/JLT.2020.2998466.

[6] Y.-W. Chen et al., "InP CDM and ICR enabled 128Gbaud/DP-16QAM-PS and 120 Gbaud/DP-QPSK long-haul transmission," *IEEE Photon. Technol. Lett.*, vol. 34, no. 9, pp. 471–474, May 2022, doi: 10.1109/LPT.2022.3165484.

[7] "Implementation agreement for micro integrated coherent receivers," OIF Implementation Agreement No. OIF-DPC-MRX-02.0, 2017. [Online]. Available: https://www.oiforum.com/wp-content/uploads/2019/01/OIF-DPC-MRX-02.0.pdf

[8] H. Yagi et al., "InP-based monolithically integrated photonics devices for digital coherent transmission," *IEEE J. Sel. Topics Quantum Electron.*, vol. 24, no. 1, Jan./Feb. 2018, Art.no. 6100411, doi: 10.1109/JSTQE.2017.2725445.

[9] Y. Ogiso et al., "80-GHz bandwidth and 1.5-V V_π InP-based IQ modulator," *J. Lightw. Technol.*, vol. 38, no. 2, pp. 249–255, Jan. 2020, doi: 10.1109/JLT.2019.2924671.

[10] Y. Ogiso, J. Ozaki, Y. Hashizume, and M. Ishikawa, "High-bandwidth InP MZ/IQ modulator PIC ready for practical use," in *Proc. IEEE Eur. Conf. Opt. Commun.*, 2022, pp. 1–3.

[11] S. Makino, S. Takeuchi, S. Maruyama, M. Doi, Y. Ohmori, and Y. Kubota, "Demonstration of thin-film lithium niobate high-bandwidth coherent driver modulator," in *Proc. IEEE Opt. Fiber Commun. Conf. Exhib.*, 2022, pp. 1–3, doi: 10.1364/OFC.2022.M1D.2.

[12] M. Xu et al., "Dual-polarization thin-film lithium niobate in-phase quadrature modulators for terabit-per-second transmission," *Optica*, vol. 9, no. 1, pp. 61–62, Jan. 2022, doi: 10.1364/OPTICA.449691.

[13] C. Wang et al., "Integrated lithium niobate electro-optic modulators operating at CMOS-compatible voltages," *Nature*, vol. 562, pp. 101–104, 2018, doi: 10.1038/s41586-018-0551-y.

[14] H. Li et al., "High performance thin-film lithium niobate MZ modulator ready for massive production," in *Proc. IEEE Opt. Fiber Commun. Conf. Exhib.*, 2022, pp. 1–3, doi: 10.1364/OFC.2022.M2D.5.

[15] M. Zhang, C. Wang, P. Kharel, D. Zhu, and M. Lončar, "Integrated lithium niobate electro-optic modulators: When performance meets scalability," *Optica*, vol. 8, no. 5, pp. 652–667, May 2021, doi: 10.1364/OPTICA.415762.

[16] J. Zhou, J. Wang, L. Zhu, and Q. Zhang, "Silicon photonics for 100 Gbaud," *J. Lightw. Technol.*, vol. 39, no. 4, pp. 857–867, Feb. 2021, doi: 10.1109/JLT.2020.3009952.

[17] Y. Shi et al., "Silicon photonics for high-capacity data communications," *Photon. Res.*, vol. 10, no. 9, pp. A106–A134, Sep. 2022, doi: 10.1364/PRJ.456772.

[18] M. Rausch et al., "A performance comparison of single-ended- and differential driving scheme at 64 Gbit/s QPSK modulation for InP-based IQ-Mach-Zehnder modulators in serial-push-pull configuration," in *Proc. IEEE Eur. Conf. Opt. Commun.*, 2015, pp. 1–3, doi: 10.1109/ECOC.2015.7341728.

[19] S. Lange et al., "Low power InP-based monolithic DFB-laser IQ modulator with SiGe differential driver for 32-GBd QPSK modulation," *J. Lightw. Technol.*, vol. 34, no. 8, pp. 1678–1682, Apr. 2016, doi: 10.1109/JLT.2015.2510228.

[20] Y. Ogiso et al., "Over 67 GHz bandwidth and 1.5 V Vπ InP-based optical IQ modulator with n-i-p-n heterostructure," *J. Lightw. Technol.*, vol. 35, no. 8, pp. 1450–1455, Apr. 2017, doi: 10.1109/JLT.2016.2639542.

[21] K. Prosyk et al., "Travelling wave Mach-Zehnder modulators," in *Proc. Int. Conf. Indium Phosphide Related Mater.*, 2013, pp. 1–2, doi: 10.1109/ICIPRM.2013.6562568.

[22] S. Akiyama et al., "InP-based Mach–Zehnder modulator with capacitively loaded traveling-wave electrodes," *J. Lightw. Technol.*, vol. 26, no. 5, pp. 608–615, Mar. 2008, doi: 10.1109/JLT.2007.915278.

[23] J. Ozaki, Y. Ogiso, Y. Hashizume, H. Yamazaki, K. Nagashima, and M. Ishikawa, "Class-80 InP-based high-bandwidth coherent driver modulator with flexible printed circuit RF interface," in *Proc. IEEE Eur. Conf. Opt. Commun.*, 2022, pp. 1–4.

[24] J. Ozaki, H. Tanobe, and M. Ishikawa, "Crosstalk reduction between RF input channels of coherent-driver-modulator package by introducing enhanced ground lead structure," *Electron. Lett.*, vol. 56, no. 17, pp. 893–1895, 2020, doi: 10.1049/el.2020.1318.

[25] J. Ozaki, Y. Ogiso, Y. Hashizume, H. Yamazaki, K. Nagashima, and M. Ishikawa, "Coherent driver modulator with flexible printed circuit RF interface for 128-Gbaud operations," *IEEE Photon. Technol. Lett.*, vol. 34, no. 23, pp. 1289–1292, Dec. 2022, doi: 10.1109/LPT.2022.3212678.

[26] Y. Ueda et al., "Compact InP spot-size converter with vertically tapered core layer formed by micro-loading effect," *Electron. Lett.*, vol. 53, no. 12, pp. 797–799, Jun. 2017.

Josuke Ozaki was born in Aichi, Japan, in 1986. He received the B.E. and M.E. degrees in engineering science from Osaka University, Osaka, Japan, in 2010 and 2012, respectively. In 2012, he joined NTT Photonics Laboratories, Japan. He is currently with the NTT Device Innovation Center. His research focuses on high-speed optical coherent driver modulators. He is a Member of the Institute of Electronics, Information, and Communication Engineers of Japan.

Yoshihiro Ogiso (Member, IEEE) was born in Fukui, Japan, in 1985. He received the B.E., M.E., and Ph.D. degrees in applied physics in optoelectronics from Waseda University, Tokyo, Japan, in 2008, 2010, and 2020, respectively. In 2010, he joined NTT Photonics Laboratories, Japan. He is currently with the NTT Device Innovation Center. His research interests include research and development of high-speed optical modulators. He is a Member of the IEEE Photonics Society.

Yasuaki Hashizume received the B.S. degree in physics from Nagoya University, Japan, in 1999, and the Dr.Eng. degree from Kyushu University, Japan, in 2015. In 1999, he joined NTT Photonics Laboratories, Japan. Since 1999, he has been developing of planar lightwave circuits. In 2014, he joined the NTT Device Innovation Center, Japan. He is a Member of the Institute of Electronics, Information and Communication Engineers of Japan.

Hiroshi Yamazaki (Member, IEEE) received the B.S. degree in integrated human studies and the M.S. degree in human and environmental studies from Kyoto University, Kyoto, Japan, in 2003 and 2005, respectively, and the Dr.Eng. degree in electronics and applied physics from the Tokyo Institute of Technology, Tokyo, Japan, in 2015. In 2005, he joined NTT Photonics Laboratories, Japan, where he has been in researching on optical waveguide devices for communications systems. He is with NTT Network Innovation Laboratories and NTT Device Technology Laboratories, Japan, where he researches optical transmission devices and systems using advanced multilevel modulation formats. He is a Member of the Institute of Electronics, Information and Communication Engineers of Japan.

Kazuya Nagashima (Member, IEEE) was born in Tokyo, Japan, in 1986. He received the B.E. and M.E. degrees from Sophia University, Tokyo, Japan, in 2009 and 2011, respectively. In 2011, he joined Furukawa Electric Co., Ltd. He has worked on development and commercialization of parallel-optical modules for optical interconnects. He is a Member of the Japan Institute of Electronics Packaging (JIEP). He was the recipient of the Best Young Researcher Award in 2015 and Best Paper Award in 2016 from the IEEE CPMT Symposium Japan, and the Best Conference Paper Award in 2016 from JIEP.

Nobuhiro Nunoya (Member, IEEE) received the B.E., M.E., and Ph.D. degrees in physical electronics from the Tokyo Institute of Technology, Tokyo, Japan, in 1997, 1999, and 2001, respectively. In 2002, he joined NTT Photonics Laboratories, Japan. From 2008 to 2009, he was with the University of California, Santa Barbara, CA, USA, where he was a Visiting Researcher. He is currently with NTT Device Innovation Center, Japan. His research interests include semiconductor lasers, semiconductor optical modulators, and integrated devices for optical communications. He is a Member of the JSAP, IEICE, and IEEE Photonics Society.

Mitsuteru Ishikawa (Member, IEEE) was born in Tochigi, Japan, in 1972. He received the B.E. and M.E. degrees in applied physics from the University of Tokyo, Tokyo, Japan, in 1995 and 1997, respectively. In 1997, he joined NTT Opto-electronics Laboratories, Japan. Since then, he has been working on research and development of semiconductor-based optical devices for WDM optical communication systems. He is a Member of the IEEE, JSAP, and IEICE.